12,05

Influence of fractality of a nickel nanonetwork on its magnetic properties

© E.V. Dvoretskaya[1], R.A. Valeev[2], M.V. Burkanov[2], R.B. Morgunov[1–3]

[1] Federal Research Center of Problems of Chemical Physics and Medicinal Chemistry RAS, Chernogolovka, Russia
[2] All-Russian Scientific Research Institute of Aviation Materials of the Research Center „Kurchatov Institute", Moscow, Russia
[3] Tambov State Technical University, Tambov, Russia

E-mail: Dvoretskaya95@yandex.ru

Received June 23, 2023
Revised June 23, 2023
Accepted August 3, 2023

The magnetic properties of a nanonetwork consisting of ultrathin Ni nanowires (diameter < 4 nm) and Ni nanoballs (diameter < 20 nm) are studied at different stages of its growth during laser ablation in a superfluid helium medium. It has been established that, at the early stages of ablation, the nanonetwork consists mainly of nanowires and has a rectangular magnetic hysteresis loop. At the late stages of ablation, the concentration of nanoballs and their diameter increase, and the shape of the hysteresis loop deviates from a rectangular one. The fractal dimension of the nanonetwork is determined, which varies from 1 in the early stages of ablation, when individual nanowires occur, to 2, when the nanonetwork becomes so dense that it is a continuous film. It is shown that the saturation magnetization changes with a change in the fractality of the nanonetwork, which, under constant ablation conditions, is explained by the transformation of nanowires into nanoballs during their folding

Keywords: Ni nanowires, laser ablation, magnetic anisotropy, fractal dimension.

DOI: 10.61011/PSS.2023.09.57120.120

1. Introduction

Magnetic nanostructures such as nanowires, nanoparticles, nanoballs [1,2] are widely used in biophysics and medicine [3–6] as well as in magnetic logic and magnetic storage devices [7]. Various nanostructures that could help overcome the discrepancy between the magnetic cell miniaturization, thermostability and data recording rate are extensively studied worldwide [8]. For example, magnetization switching by electric field or light is offered — one of possible ways to overcome this trilemma [9,10]. Moreover, magnetic nanonetworks having fractal dimensions and properties that are much different both from single nanoballs and single nanowires [11–13]. Ferromagnetic nanowires that form a nanonetwork demonstrate multiple stable energy minima with corresponding values relative to stable magnetic moments [14]. Interaction of nanonetwork components — nanowire segments — is the main advantage and underexplored property of nanonetworks. magnetization transfer and transmission between the segments are carried out by means of domain wall displacement and dipole-dipole interaction that generally makes the system rather complex. Magnetization transfer between nanowire segments makes it possible to create neurophysical system simulators [15,16]. In particular, antiferromagnetic/ferromagnetic heterostructures were used to implement an artificial neuron and synapse [17] that, when included in a magnetic nanonetwork, may work as a single neuronetwork. Magnetic interactions and multiple stable states of the artificial nanonetwork may be used to create artificial intelligence. Galvanic signal in the presence of magnetoresistance can be encrypted using magnetic network components [15,16]. In biology, magnetic nanonetworks are used to filter few magnetically labelled cells in order to separate them from the mixture of cells of various types [18].

This study uses nanonetworks that, when the overlapping nanowire segments are elongated beoynd the critical dimension, are transformed by rolling nanowires into globules that finally form nanoballs. We have shown in [14] that under constant nickel ablation conditions in liquid helium at late nanonetworking stages, the anisotropy constant varies. The anisotropy constant mainly corresponds to nanoballs that make a greater contribution to the anisotropy than nanowires. Formation of globules (nanoballs) enables the information to be written into the structure with light remagnetization (individual nanowires) and stored in a structure with hard demagnetization (nanoballs). This may be addressed as a way to overcoming the magnetic trilemma that restricts the increase in density and writing rate, while maintaining or increasing the data storage time at the same tome.

The objective of this work was to analyze the fractal dimension of the nanonetwork at different stages of its formation from individual nanowires to a continuous film and to establish the influence of the topological parameters of the nanonetwork on its magnetic properties.

2. Samples and methods

The nanonetwork was created by means of laser ablation in superfluid helium atmosphere (He II), where quantum

vortices, as described in detail in [19,20]. Diameter of the produced transition metal nanowires is $\sim 2-5$ nm [21,22]. Nanowire segments intersect and form a network containing nanoballs on a silicon substrate whose diamagnetic contribution was subtracted.

At the initial stage with low Ni concentration, a group of individual nanowires was observed, while with increasing ablation time nanowire concentration grows and then these nanowires form the nanonetwork. At the late ablation stage, when Ni concentration becomes high, nanowires are rolled into globules (nanoballs). For morphological analysis of the produced nanonetwork, the network was deposited in the TEM (Transmission electron microscopy) grid covering the $1 \times 1 \times 4\,\text{mm}^3$ silicon substrate. Morphological, microstructure and local elemental analysis of the nanonetwork was carried out using JEM-2100 transmission electron microscope (TEM) and Zeiss Supra 25 scanning election microscope (SEM) with energy-dispersive microanalysis (EDX).

The magnetic moment of a nanonetwork applied to the silicon substrate was measured using MPMX 5XL Quantum Design SQUID-magnetometer at different structure formation stages. The magnetic moment of a single nanoball was recorded using an Integra Aura NT-MDT atomic-force microscope with a silicon-based ferromagnetic cantilever coated with a thin CoCr film. Sample surface scanning was performed by the two-pass method: the first cantilever pass above the sample recorded the surface profile (AFM), and the second pass recorded the magnetic force distribution in the sample (MFM).

3. Experimental findings

EDX spectrum of a single Ni nanoball shows content 99% of Ni and 1% of O in the test sample, and the Si peak corresponds to the Si-substrate (Figure 1, *a*). In the SEM image of a single nanoball (inset 1, *a*), nanowires forming the nanoball can be distinguished.

Nanonetwork evolution was observed with increasing laser ablation time and the amount of Ni directly proportional to the time. For this, TEM images of the network without balls at the early 10-minute ablation stage (inset 1, *b*) and of the nanonetwork at a later 20–60-minute ablation stage (inset 1, *c*) were compared. The electron diffraction patterns of the nanonetwork segments consisting of nanowires (inset 1, *b*) and nanoballs (inset 1, *c*) show that nanowires have a heavily disordered amorphous structure, while nanoballs have a polycrystalline structure. Statistical processing covered 2200 TEM images of free nanowire segments and 65 nanoballs. Thus, distributions of free Ni nanowire segment lengths and of nanoball diameters were built and these parameters were found to have lognormal distribution (solid lines in Figure 1, *b, c*).

Magnetic hysteresis loops at 300 K and by parallel orientation of the external magnetic field relative to the Si-substrate with Ni products at various laser ablation stages are shown in Figure 2. It is apparent that the magnetic moment of the nanonetwork M increases with the ablation

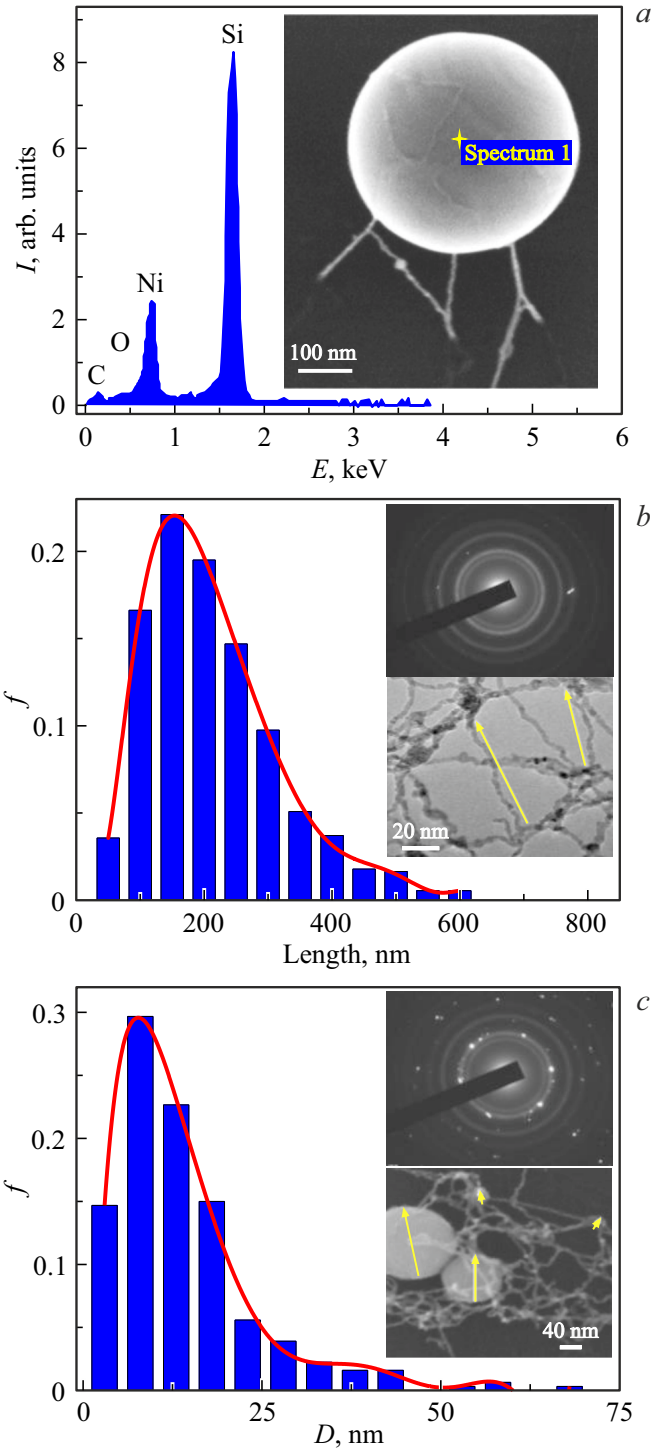

Figure 1. *a* — EDX spectrum of a single nanoball. The inset shows a SEM image of a single nanoball formed by nanowires. *b* — distribution of free nanowire segment lengths normalized to the total number of nanowires at the early ablation stage. The inset shows electron diffraction pattern of the sample and TEM image of Ni nanowires at the early ablation stage (free sections of nanowires are shown by arrows). *c* — distribution of nanoball diameters normalized to the total number of nanoballs in the sample. The inset shows electron diffraction pattern and TEM image of the nanonetwork consisting of nanowires and nanoballs at the late ablation stage (nanoball diameters are shown by arrows).

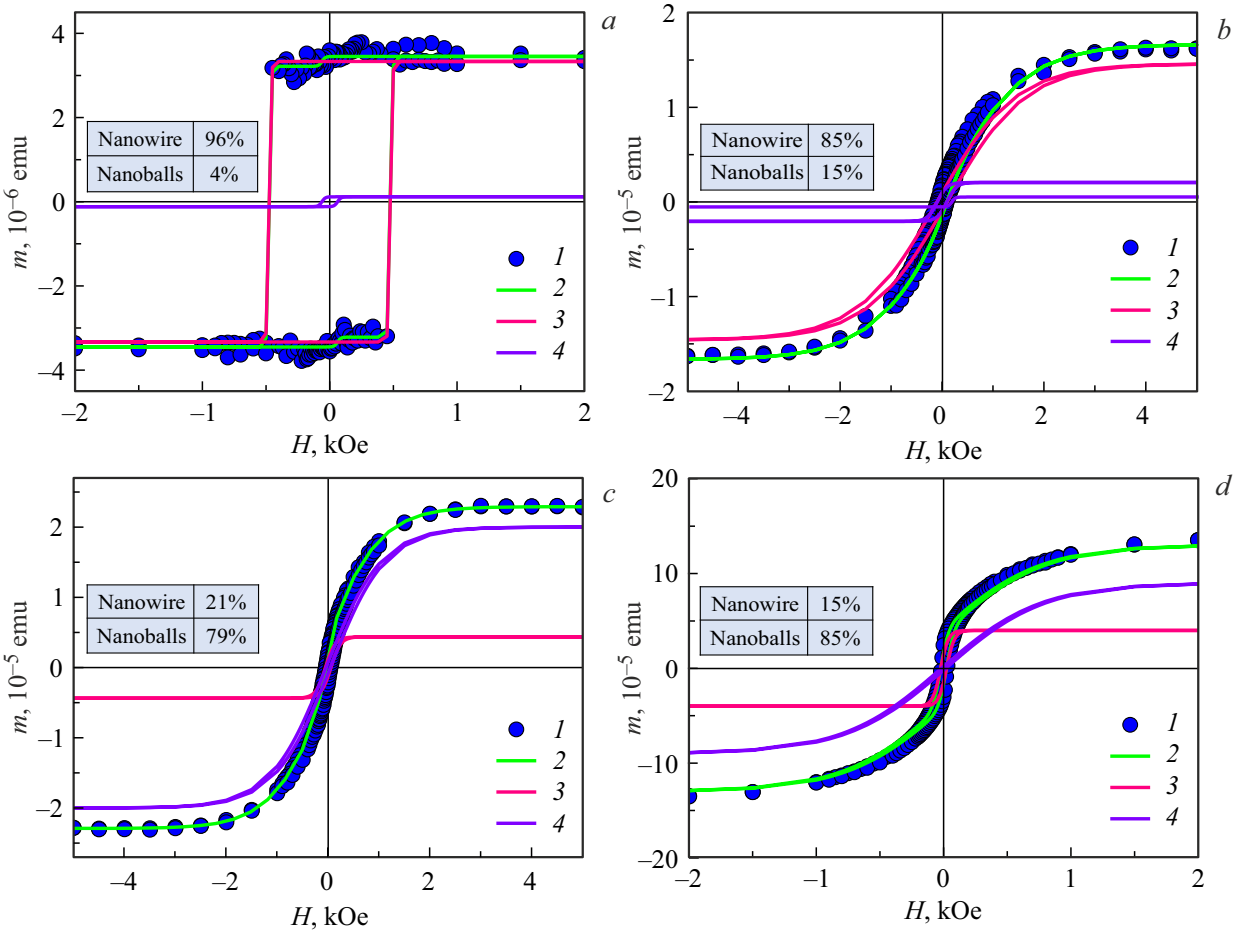

Figure 2. Magnetic hysteresis at 300 K: *a* — in a sample with low Ni concentration after short-term laser exposure 10 min; *b* — in a sample with intermediate Ni concentration after laser exposure 20 min; *c* — in a sample with Ni concentration higher than the average level after laser exposure 30 min; *d* — in the sample with high Ni concentration after laser ablation during 60 min. Blue symbols (*1*) — experimental data; solid green lines (*2*) — approximation by two hysteresis. Individual magnetic contributions of nanowires and nanoballs are shown by thin solid pink (*3*) and purple (*4*) lines, respectively. Relative volume concentrations of nanowires and nanoballs are shown in the respective Figures.

time that is explained by the growing amount of Ni with increasing ablation time.

It is apparent that at the initial stage, when mainly nanowires are present in the sample, the hysteresis loop is rectangular, and at later stages, when nanoballs occur, the loop is inclined. Assuming that the rectangular component is assigned to nanowires, while the inclined component is assigned to nanoballs, and assuming that the hysteresis loop parameters of these components are unchanged during the ablation process, the experimental hysteresis loops were approximated by two contributions (shown by lines *3* and *4* in Figure 3) and the relative volume content of nanowires and nanoballs was determined at various ablation stages (see the Tables in insets in Figure 2, *a*–*d*). It is apparent that nanoballs start prevailing with growing ablation time. Saturation magnetic moment m_s vs. ablation time for the whole nanonetwork *1*, for nanowires *2* and nanoballs *3* is shown in Figure 3. Straightening these dependences in double logarithmic coordinates indicates a power-law dependence of the magnetic moment on time $m(t) \sim t^n$ with different n values for nanowires and nanoballs. This indicates the diffusion nature of the growth of nanowires and nanospheres.

For further analysis and separation of the nanoball and nanowire contributions, magnetization of a single nanoball was examined in detail. Images of a single nanoball were recorded in magnetic force microscopy (MFM) and atomic-force microscopy (AFM) modes (insets in Figure 4, *a*, respectively). The MFM mode measures the magnetic moment of a single nanoball μ, because the measured magnetic force is proportional to the second magnetic field derivative near the test sample surface [23]. Local distribution of the single nanoball scattering field was scanned in a semicontact mode at different heights h between the sample surface and cantilever tip, while the microscope response was proportional to the phase shift of the vibrating cantilever. In the MFM mode, the phase shift was recorded as function of position, and in the AFM mode, the cantilever height above the surface was scanned (Figure 4, *a*, respectively).

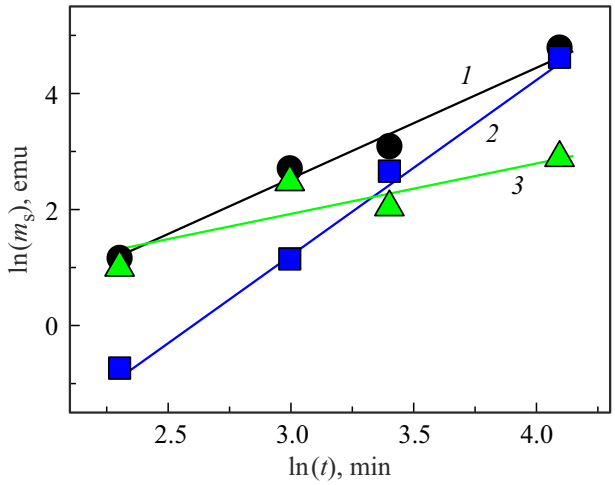

Figure 3. Saturation magnetic moment m_s vs. ablation time for whole sample (*1*), for nanoballs (*2*) and nanowires (*3*).

Similar measurements were made on a series of nanoballs with different diameters. As a result, the dependence of phase shift $\Delta\phi$ vs. nanoball diameter d (Figure 4, *b*) was obtained. This dependence was used to calculate the magnetic moment of a single ball with the pre-defined diameter. The local scattering field of a single Ni nanoball is equal to the scattering field of a point dipole located in the center of the nanoball. Phase shift $\Delta\phi$ of the vibrating cantilever was calculated as follows

$$\Delta\phi = \frac{M_S \pi d^3}{6c(h)}, \qquad (1)$$

where $c^{-1}(h)$ is an unknown coefficient of proportionality [23]. According to the calibration algorithm offered in [23], the coefficient of proportionality $c(h)$ was calculated. Constant $c = 0.04\,\mathrm{A}\cdot\mathrm{nm}^2$ was derived from the dependences of the phase shift $\Delta\phi$ on the nanoball diameters d at $h = 50\,\mathrm{nm}$ (Figure 4, *b*). Thus, the appropriate magnetic moment $\mu = 4.5\cdot10^{-19}\,\mathrm{A}\cdot\mathrm{m}^2$ of a single nanoball $d = 75\,\mathrm{nm}$ was measure experimentally and agreed closely with the theoretically calculated $\mu = M_S\pi d^3/6 = 4.2\cdot10^{-19}\,\mathrm{A}\cdot\mathrm{m}^2$ of the single-domain nanoball $d = 75\,\mathrm{nm}$ at the tabular Ni saturation magnetization values M_S.

4. Discussion

It is well known from the literature that amorphous nano- and microwire are magnetically bistable provided that they have a single-domain magnetic structure [24,25]. Bistability is defined by the rectangular hysteresis loop of the sample with parallel orientation of the external magnetic field. This means that magnetization of the nano- and microwire changes its direction sharply with the external field polarity reversion [25].

When addressing the magnetic properties of the Ni nanonetwork, two aspects were considered: 1) nanonetwork contains a lot of nanowire segments that may be with equal probability both parallel and perpendicular to the external magnetic field. When the external field sign is reversed, magnetization will change rapidly only in the segments that are parallel to the field; 2) the nanonetwork can be

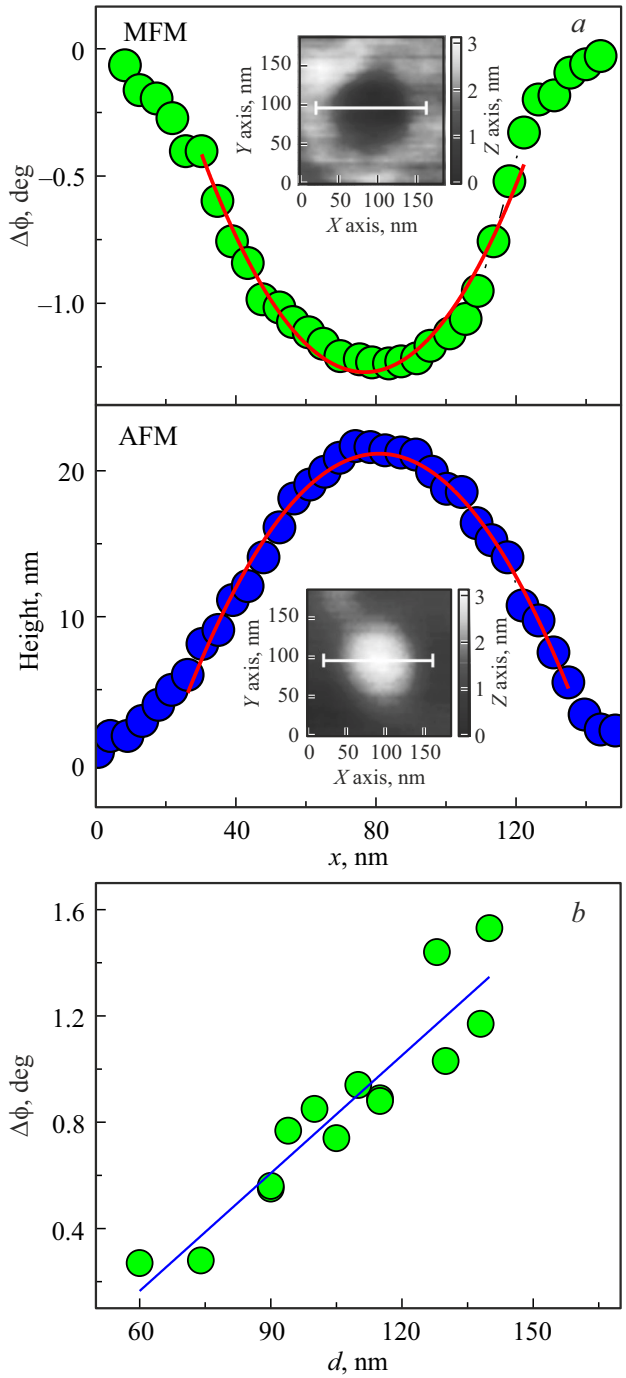

Figure 4. *a* — phase contrast profiles of the Ni nanoball recorded in MFM mode (cantilever vibration phase variation $\Delta\phi$) and AFM mode (geometrical profile height of the particle). Corresponding Ni nanoball images are shown in the insets; *b* — phase shift $\Delta\phi$ vs. nanoball diameter d with the same distance between the nanoball surfaces and cantilever ($h = 50\,\mathrm{nm}$). Solid line shows the linear approximation.

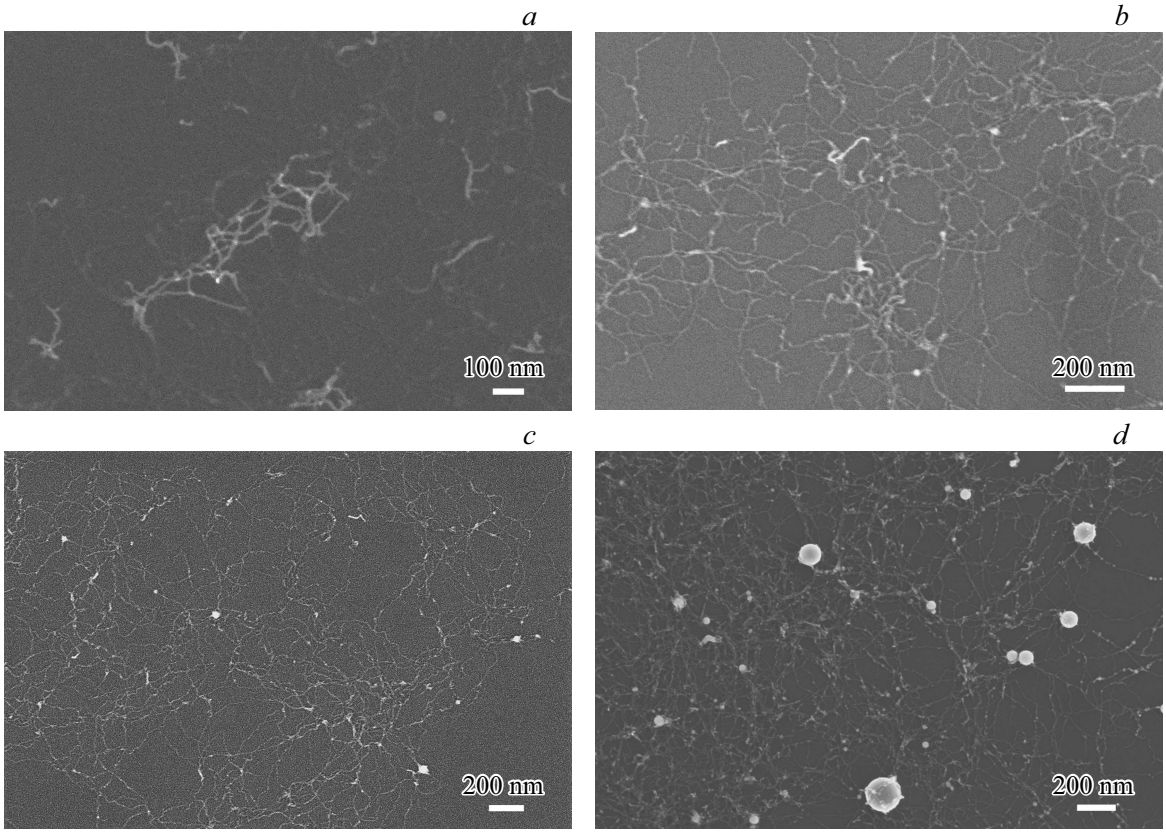

Figure 5. SEM images of the Ni nanonetwork after 10 min (*a*), 20 min (*b*), 30 min (*c*), 60 min (*d*) ablation.

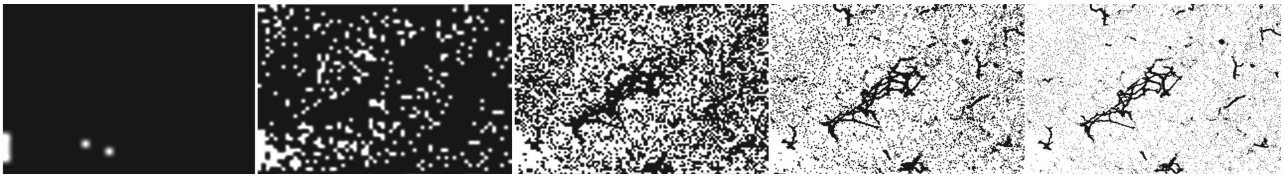

Figure 6. Successive local adaptive binarization frames of the SEM image of the Ni nanonetwork after 10 minute ablation.

considered as a thin, continuous film of nickel, the axis of easy magnetization of which is located in its plane.

The experimental data in Figure 2 (blue symbols) show clearly how the ablation time influences the saturation magnetization M_S and coercive force H_C in the Ni nanonetwork. With increasing ablation time, M_S increases, the hysteresis loops inclines and H_C decreases. The model of two independent hystereses described in [24] allows one to simultaneously take into account the contribution of both nanowires and nanospheres, which correspond to the indices $i = 1$ and $i = 2$ when expanding the hysteresis loops of a nanonetwork

$$m(H) = \sum_{i=1}^{2}\left(m_S^i - \frac{2m_S^i}{1 + \exp((H \pm H_C^i)/p^i}\right), \qquad (2)$$

where m_S^i are component saturation magnetizations, H is the external magnetic field, signs „+“ and „–“ are descending and ascending portions of the hysteresis loop, respectively, H_C^i is the coercive force of nanowires and nanoballs, respectively, p^i is the hysteresis loop squareness ratio for nanowires ($p^1 = 0.95$) and nanoballs ($p^2 = 0.45$), respectively.

In Figure 2, green lines a represent approximations by expression (2) of experimental data (blue — symbols), and pink and purple lines correspond to the rectangular component of the hysteresis loop recorded from nanowires and to the inclined component recorded from nanoballs. In the insets in Figure 2 show relative volume fractions at various ablation stages for nanowires and nanoballs included in the nanonetwork that were calculated with demagnetization factors 2/3 or the ball and 2π for the wire treated as a cylinder. The foregoing suggests that the hysteresis loop squareness decreases with increasing number of nanoballs in the Ni nanonetwork.

The weight of the nanonetwork applied to the Si-substrate is many times lower than that of the Si-substrate and is

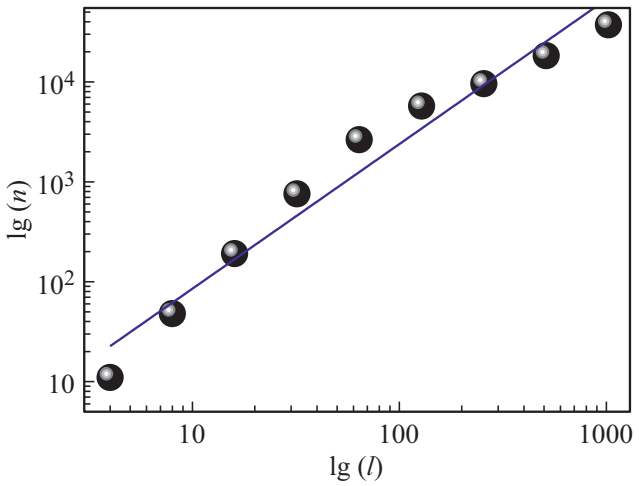

Figure 7. Double logarithmic dependence of the number of black pixels n (objects) on the mesh size l of the grid covering the object for the Ni nanonetwork after 10 min laser ablation. Solid line shows the power law with exponent $d = 1.24$.

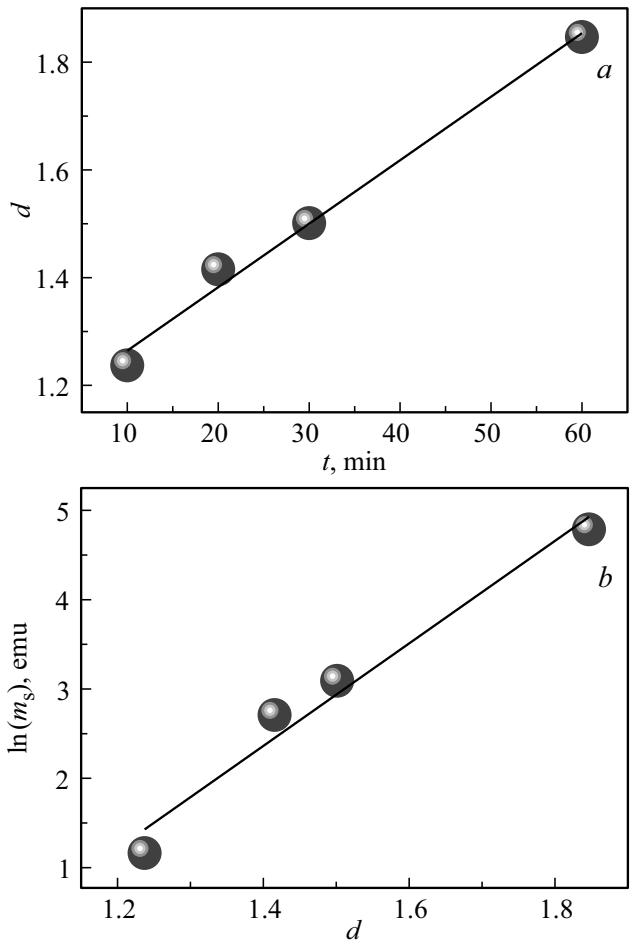

Figure 8. a — time dependence of he fractality exponent d of the Ni nanonetwork; b — dependence of the saturation magnetic moment M_s on the fractality exponent for Ni nanonetwork at various ablation stages.

not available for direct measurements. Therefore, $m_S(t)$, whose growth (Figure 3, *b*, curve *1*) is, in turn, directly attributable to the increasing amount of Ni with ablation time, is the only method that can be used to determine the amount of Ni. Such assumption is true based on the fact that Ni saturation magnetization $M_S = 58.6$ emu/g (522 emu/cm^3) is well known [26]. According to the percentage ratio of nanoball and nanowire volumes at various ablation stages, respective dependences $m(t)$ were built for nanoballs and nanowires (Figure 3, *b*, curves *2* and *3*). According to the previous data, the number and size of Ni nanoballs increase with increasing laser ablation time and make the main contribution to the magnetic moment m of the Ni nanonetwork built at later laser ablation stages. Straightening of curves *1–3* in Figure 3, *b* in $\ln(m) - \ln(t)$ positions follows the exponential function $m(t)$: $m \sim t^n$, $n = 1.36 > 1$ for the whole sample. The power law corresponds the state when there is a dependence between the magnetic properties and size of the system as for the expected linear increase of the amount of Ni with laser ablation time. The superlinear dependence $m(t)$ is caused by gradual variation of the percentage ratio of Ni nanowires and Ni nanoballs as well as Ni network formation.

The nanonetwork in the SEM images may be described as a fractal (Figure 5) by determining its fractal dimension at different ablation stages.

Ni nanonetwork images were analyzed using Wolfram Mathematica software. To separate the grayscale images into „objects“ and „background“ local adaptive binarization (conversion into a two-color black-and-white image) was applied to the image at the first stage. Such method takes into account the color of adjacent pixels for each image pixel allowing to preserve small nanowires as much as possible („object“ painted black) cutting off the „background“ painted white (Figure 6).

To determine the fractal dimension, a square grid with different mesh sizes was applied to the binary SEM image of the nanonetwork in Wolfram Mathematica software and the number of meshes in the grid occupied by the „object“ was determined. For d-size object, the number of squares n occupied by the object will be proportional to the grid mesh size l: $n \sim l^d$. For fractal objects, d is a non-integer. Dependence of the number of black pixels n (objects) on the grid mesh size l covering the object was obtained (Figure 7). This dependence is well straightened in logarithmic coordinates and is a power function with an exponent $d = 1.24$ for the Ni nanonetwork after 10 minute ablation.

From the SEM images of the nanonetwork (Figure 5), fractality exponents $d = 1.42$, $d = 1.5$, $d = 1.85$ for 20, 30 and 60 min ablation, respectively, were obtained using the fractal dimension calculation software. Figure 8 shows the fractality exponent vs. ablation time (Figure 8, *a*) and magnetic moment m_s of the nanonetwork vs. fractality exponent for the Ni nanonetwork at various ablation stages (Figure 8, *b*).

The fractality exponent increases from $n = 1.24$ for 10 minute ablation to $n = 1.85$ for 60 minute ablation that

should be expected with increase in the number of Ni nanowires in the nanonetwork. Straightening of $\ln m_s(d)$ is indicative of rapid exponential growth of the magnetic moment with increasing fractal dimension. This may be explained by the fact that each new emerging nanonetwork component is an inoculant for the accelerated growth and deposition of Ni on it.

5. Conclusions

1. Increasing laser ablation time results in formation of polycrystalline Ni nanoballs built in the nanonetwork from nanowires. The diameter and number of balls grow with increasing ablation time. In this case, the growth of the magnetic moment is described by a superlinear power-law dependence, characteristic of diffusion processes.

2. By way of analysis of the magnetic properties of the Ni nanonetwork at various ablation stages, contribution of nanowires and nanoballs to the magnetic moment of the nanonetwork was established. Nanowires are characterized by the ideal square hysteresis loop and nanoballs have the inclined hysteresis loop shape.

3. The Ni nanonetwork is a fractal structure forming in several stages with gradually increasing fractality exponent with increase of Ni in the nanonetwork. From the SEM images of the Ni nanonetwork it was found that Ni nanowires are the main components forming the fractal structure. By varying the ablation time, self-similar structures with the required shape and pre-defined magnetic properties may be controlled and built.

Funding

The study was carried out as part of the thematic map of the Federal Research Center for Problems of Chemical Physics and Medical Chemistry, RAS, AAAA-A19-119092390079-8.

Conflict of interest

The authors declare that they have no conflict of interest.

References

[1] E.C. Stoner, E.P. Wohlfarth. A mechanism of magnetic hysteresis in heterogeneous alloys. Philosophical Transactions of the Royal Society of London. United Kingdom, London (1948). P. 599–642.
[2] S.A. Nepijko, R. Wiesendanger. SPQEO **2**, *5*, 9 (1999).
[3] A. Akbarzadeh, M. Samiei, S. Davaran. Nanoscale Res. Lett. **7**, 144 (2012).
[4] S.K. Murthy. Int. J. Nanomedicine **2**, *2*, 129 (2007).
[5] S.P. Gubin, Y.I. Spichkin, G.Y. Yurkov, A.M. Tishin. Russ. J. Inorg. Chem. **47**, *1*, 32 (2002).
[6] P. Malik, S. Pandya, V. Katyal. IJAR **1**, *1*, (2013).
[7] S. Karmakar, S. Kumar, R. Rinaldi, G. Maruccio. J. Phys. Conf. Ser. **292**, 012002 (2011).
[8] R.C. O'Handley. Modern magnetic materials: principles and applications. Wiley, N.Y., USA (2000). 768 p.
[9] C.-H. Lambert, S. Mangin, B.S.D.Ch.S. Varaprasad, Y.K. Takahashi, M. Hehn, M. Cinchetti, G. Malinowski, K. Hono, Y. Fainman, M. Aeschlimann, E.E. Fullerton. Science **345**, 1337 (2014).
[10] J. Hohlfeld, Th. Gerrits, M. Bilderbeek, Th. Rasing, H. Awano, N. Ohta. Phys. Rev. B **65**, 012413 (2001).
[11] D. Bürger, S. Zhou, M. Höwler, X. Ou, G.J. Kovacs, H. Reuther, A. Mücklich, W. Skorupa, H. Schmidt. Springer International Publishing Switzerland **192**, 15 (2014).
[12] Y. Lin, S. Zhou, S.W. Sheehan, D. Wang. J. Am. Chem. Soc. **133**, *8*, 2398 (2011).
[13] E. Saitoh, M. Tanaka, H. Miyajima, T. Yamaoka. J. Appl. Phys. **93**, 7444 (2003).
[14] S. Labbé, Y. Privat, E. Trélat. J. Differ. Equ. **253**, *6*, 1709 (2012).
[15] C. Kittel. Phys. Rev. **70**, 965 (1946).
[16] F. Vajda, E.D. Torre. J. Appl. Phys. **73**, 5833 (1993).
[17] A. Kurenkov, S. DuttaGupta, C. Zhang, S. Fukami, Y. Horio, H. Ohno. Adv. Mater **31**, 1900636 (2019).
[18] C. Lai, W. Tsai, M. Yang, T. Chou, Y. Chang. Nanoscale **11**, 21119 (2019).
[19] E.B. Gordon, R. Nishida, R. Nomura, Y. Okuda. JETP Lett. **85**, 581 (2007).
[20] D. Mateo, J. Eloranta, G.A. Williams. J. Chem. Phys. **142**, 064510 (2015).
[21] E.B. Gordon, A.V. Karabulin, V.I. Matyushenko, V.D. Sizov, I.I. Khodos. J. Exp. Theor. Phys. **112**, 1061 (2011).
[22] E.B. Gordon, M.E. Stepanov, M.I. Kulish, A.V. Karabulin, V.I. Matyushenko, I.I. Khodos. Laser Phys. Lett. **16**, 026002 (2019).
[23] S. Sievers, K.-F. Braun, D. Eberbeck, S. Gustafsson, E. Olsson, H. Werner Schumacher, U. Siegner. Small **8**, 2675 (2012).
[24] F. Tian, Z.P. Huang, L. Whitmore. Phys. Chem. Chem. Phys. **14**, 8537 (2012).
[25] K.M. Razeeb, F.M.F. Rhen, S. Roy. J. Appl. Phys. **105**, 083922 (2009).
[26] H. Danan, A. Herr, A.J.P. Meyer. J. Appl. Phys. **39**, 669 (1968).

Translated by E.Ilyinskaya